ACS APPLIED BIO MATERIALS

www.acsabm.org
Article

Mechanical and Electrical Properties of Red Blood Cells Under Oxidative Stress Using Optical Tweezers

Theodoros Giannakis, Sotirios P. Fortis, Maria-Aspasia Kosma, Evangelos Meletis, Anastasios G. Kriebardis, and Maria Kandyla*

Cite This: https://doi.org/10.1021/acsabm.6c00869

ABSTRACT: Red blood cells (RBCs) rely on their mechanical and electrostatic properties to maintain microvascular circulation and oxygen delivery. Oxidative stress, a hallmark of many diseases, disrupts these properties by damaging membrane lipids and cytoskeletal proteins. In this study, RBCs from healthy donors were incubated with three oxidative agents, i.e., phenylhydrazine (PHZ), *tert*-butyl hydroperoxide (t-BHP), and diamide, to investigate how oxidative stress affects the combination of single-cell mechanical, morphological, biochemical, and electrical properties under different oxidizing conditions. All oxidants significantly increased intracellular reactive oxygen species (iROS), with PHZ producing the strongest effect. Morphological analysis revealed acanthocyte and echinocyte formation and a reduced cell diameter. Zeta potential (ζ) remained unchanged across treatments when measured in phosphate-buffered saline (PBS) solution, suggesting a preserved surface charge under these conditions. Mechanical properties were assessed by optical tweezers at the single-cell level to estimate overall elasticity and bending modulus. Untreated and t-BHP-treated RBCs showed comparable elasticity and bending modulus. Diamide increased overall elasticity and slightly elevated bending modulus, while PHZ severely impaired elongation capability, inducing an irregular trapping behavior and prohibiting the calculation of the bending modulus. These findings demonstrate that oxidative stress exerts agent-specific effects on RBC biomechanics, with t-BHP inducing mild alterations, diamide increasing elasticity, and PHZ causing profound damage. To our knowledge, this is the first study to directly correlate oxidative damage, mechanical stiffness, and electric properties across single-cell and population scales, providing a comprehensive evaluation of RBC responses to oxidative injury.

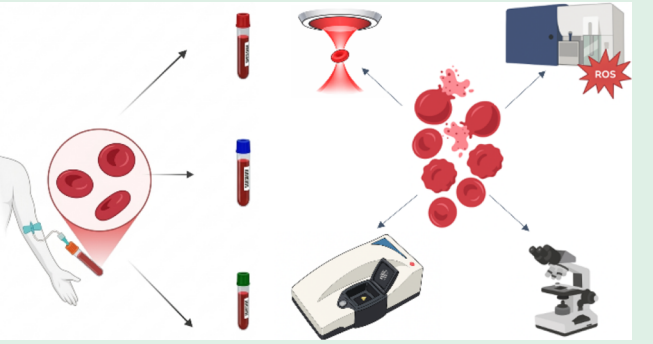

KEYWORDS: *red blood cells, oxidative stress, optical tweezers, optical trapping, mechanical properties, electrical properties, ζ-potential, bending modulus*

1. INTRODUCTION

Red blood cells (RBCs) are the most common blood cell type and they are highly specialized for oxygen and carbon dioxide transport throughout the human body.[1] During their ~120-day lifespan, RBCs travel approximately 300 km within the human circulation[2] and their ability to traverse the microvasculature network depends strongly on their mechanical properties.[3] Parameters such as cell elasticity,[4] bending modulus,[5] surface charge (zeta potential, ζ),[6] and viscoelastic response govern how RBCs deform under shear flow, squeeze through capillaries narrower than their own diameter, and avoid aggregation. Alterations in these properties can impair oxygen delivery, increase hemolysis, or lead to vascular complications.[7] Therefore, understanding the intrinsic biomechanical characteristics of RBCs at the single-cell level is critical not only for fundamental hematology but also for assessing how factors such as storage-induced damage[8,9] or inherited disorders like β-thalassemia[10] can alter their mechanical performance and contribute to clinical complications.

Oxidative stress in RBCs refers to an imbalance between reactive oxygen species (ROS) production and antioxidant defenses. It is a common pathological feature in diseases such as diabetes, sickle cell anemia, malaria, cardiovascular disorders, and Parkinson's disease.[11] It occurs when excessive ROS production or insufficient antioxidant capacity disrupts RBC homeostasis, leading to oxidative damage of membrane lipids,[12]

Received: May 2, 2026
Revised: July 27, 2026
Accepted: August 7, 2026

hemoglobin,[13] and cytoskeletal proteins,[14] which ultimately impairs whole-cell deformability, accelerates RBC aging, and compromises microvascular oxygen delivery.[15] Studying how oxidative stress affects the mechanical and electrostatic properties of RBCs helps clarify the link between biochemical damage and biomechanical dysfunction, particularly regarding the alteration of RBC membrane deformability under oxidative conditions.[16] This approach is particularly valuable because it can simulate cellular aging or disease-related damage in a controlled setting, providing mechanistic insights into how RBC properties deteriorate under pathological conditions.[17] Oxidative stress in RBCs can be experimentally induced using common oxidizing agents such as phenylhydrazine (PHZ),[18] *tert*-butyl hydroperoxide (t-BHP),[19] and diamide.[20,21] t-BHP induces oxidative damage mainly through lipid peroxidation and secondary membrane protein oxidation, leading to membrane rigidification.[22] Diamide oxidizes protein thiols and disrupts membrane−cytoskeleton interactions, while PHZ causes hemoglobin denaturation and band 3 clustering, resulting in membrane destabilization and senescence-like changes.[23]

Several well-established biophysical techniques are available for quantifying the mechanical properties of RBCs, including optical tweezers,[24] atomic force microscopy (AFM),[25] micropipette aspiration,[26] ektacytometry,[27] magnetic twisting cytometry,[28] oscillatory rheology,[27] and others. Among these, optical tweezers offer the distinct advantages of non-contact, highly localized manipulation of single cells with piconewton force sensitivity[29] and minimization of mechanical artifacts introduced by probes or surfaces. In contrast to bulk methods, optical tweezers allow precise control over cell orientation and enable dynamic measurements under physiologically relevant conditions.[30] Furthermore, they permit simultaneous imaging and mechanical probing, facilitating direct correlation between morphological changes and mechanical response. These features render optical tweezers particularly powerful for studying subtle alterations in RBC biomechanics at the single-cell level.[31] Optical tweezers have been successfully employed to investigate changes in the elasticity of healthy RBCs, with particular emphasis on the effects of storage in blood bags.[32] Furthermore, several optical tweezer studies have explored the influence of pathological conditions on RBC mechanics, such as β-thalassemia,[10] leptospirosis,[33] sickle cell anemia,[34] and malaria,[35] or the effect of exposure to ionizing radiation.[36]

Optical tweezers have been employed to some extent to measure electric or mechanical changes in RBCs under oxidative stress, mainly induced by hydrogen peroxide (H_2O_2). The impact of oxidative stress on the shear modulus of RBCs has been investigated using dual-beam optical trapping in cells treated with H_2O_2 and the membrane shear modulus was found to increase with H_2O_2 concentration.[11] Dual-beam optical tweezers, combined with digital holographic microscopy, have also been employed to investigate oxidative stress-induced changes in RBCs, enabling simultaneous quantification of microdeformation, mechanical stiffening, and morphological alterations following H_2O_2 treatment.[37] Single-beam Raman tweezers have been used to characterize chemically-induced oxidative stress in optically trapped RBCs and distinguish stressed from normal ones at the biochemical level.[38] Dielectrophoretic force measurements with an optical tweezer-assisted microfluidic platform have demonstrated altered electrical properties under H_2O_2-induced oxidative stress on RBCs.[39] While these studies demonstrate the value of optical tweezers in assessing H_2O_2-mediated changes at the single cell level, they typically focus on a single oxidizing agent and an isolated physical parameter. Consequently, how distinct biochemical pathways of oxidative stress differentially alter the coupled physiological properties of RBCs remains an open question.

In this work, we address this remaining question by introducing a comprehensive, multi-parameter framework that directly compares three distinct oxidative agents (PHZ, t-BHP, and diamide, each representing a unique mechanism of oxidative injury) and evaluate their effect on the combination of mechanical, morphological, biochemical, and electrical properties of RBCs. We expose healthy RBCs to these three oxidative agents and evaluate the intracellular ROS (iROS) production, membrane morphological changes, overall elasticity, bending rigidity, and membrane electric charge. We employ optical tweezers to probe the RBC mechanical properties and bending behavior at the single-cell level, enabling precise quantification of bending modulus and overall elasticity, while population-based techniques, including flow cytometry and electrophoretic measurements, provide complementary biochemical and electric information. To the best of our knowledge, this is the first study to directly correlate oxidative damage, mechanical stiffness, and electrical properties across single-cell and population scales. All oxidants significantly increase iROS, with PHZ producing the strongest effect. Our findings indicate that diamide induces a measurable increase in membrane stiffness and a slightly elevated bending modulus with subtle morphological changes, t-BHP causes minimal mechanical alterations, and PHZ leads to severe structural damage and irregular mechanical behavior. These results reveal that RBC mechanical responses are tightly coupled to the degree and type of oxidative injury. Zeta potential measurements suggest preserved surface charge across treatments, when evaluated in a phosphate-buffered saline (PBS) solution. By capturing these disparate cellular properties simultaneously across scales, this comprehensive approach allows us to uncover mechanistic relationships that cannot be resolved using isolated, individual techniques alone.

2. MATERIALS AND METHODS

2.1. Optical Tweezers

The custom-built optical trapping apparatus (Figure 1) employed a continuous-wave (CW) diode-pumped solid-state laser with a wavelength of 1064 nm. This wavelength is widely regarded as optimal for trapping biological samples because it minimizes photothermal and photochemical damage while maintaining high trapping efficiency.[40] The linearly polarized laser beam was routed through a half-wave plate ($\lambda/2$) and polarizer assembly, allowing fine control of the output power. Following power adjustment, the beam was expanded by a factor of four using a Keplerian telescope (L2-L3) to overfill the back aperture of the objective lens, thereby maximizing the optical gradient forces. The beam was then tightly focused onto the sample chamber using a 100× oil-immersion objective lens with a numerical aperture (NA) of 1.25, providing the high spatial confinement required for stable trapping of a single RBC. The sample chamber consisted of an Improved Neubauer chamber (depth = 100 μm), sealed with a cover glass slide, and contained RBCs suspended in plasma solution (Inset Figure 1). For real-time observation of trapped cells, an inverted white-light transmission microscope was integrated into the optical tweezer setup, equipped with a cold white LED source, a 10× condenser lens (NA = 0.25), and a high-sensitivity CMOS camera operating at 25 frames per second. The sample chamber was mounted on a computer-controlled three-axis (*xyz*) translation stage, which provides

https://doi.org/10.1021/acsabm.6c00869
ACS Appl. Bio Mater. XXXX, XXX, XXX−XXX

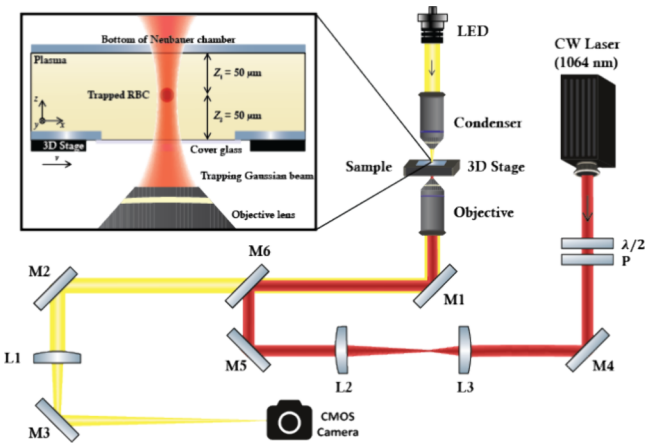

Figure 1. Schematic representation of the optical trapping experimental setup. M1-M5, mirrors; M6, broadband dielectric mirror; L1-L3, lenses; λ/2, half-wave plate; P, polarizer. Inset: schematic representation of a trapped RBC in plasma solution inside the Neubauer chamber.

precise positioning of the chamber, enabling controlled manipulation and measurements at the single-cell level. The resolution of the three-axis translation stage is 1.25 μm. Laser-induced oxidative stress in the trapping apparatus is excluded in this work due to the low power of the trapping laser and the brief RBC measurement time. Indeed, it has been shown that, at 1064 nm, a laser power below 20 mW causes only transient, fully reversible hemoglobin deoxygenation.[41] Irreversible effects, such as singlet-oxygen-driven protein cross-linking and hemoglobin aggregation, require significantly higher powers and continuous exposure of cells for at least 5 min, which exceeds the measurement window of 2–3 min per cell employed here. Indeed, optical trapping measurements in the control group of untreated RBCs did not demonstrate laser-related oxidizing effects.

2.2. RBC Samples

Peripheral whole blood samples were obtained from ten healthy donors (n = 10; 3 males and 7 females; mean age: 21.6 years). All donors provided written informed consent, and the study was conducted in accordance with a protocol approved by the Research Ethics Committee of the National and Kapodistrian University of Athens (see Ethics Statement). The samples were washed three times with PBS (310 mOsm) containing 1% glucose. Packed RBCs were diluted 1:1 with PBS-glucose solution and a 5.5-μL aliquot of each sample was diluted in the same PBS-glucose buffer. Oxidative stress was induced by incubating RBCs at 37 °C with three different oxidative agents: PHZ (100 μM), t-BHP (100 μM), and diamide (2 mM).[23] Control samples were treated with PBS-glucose only. Following incubation, RBCs were washed and adjusted to a final hematocrit of 4%.

Samples were prepared in three groups to separately assess plasma viscosity, RBC viscoelastic properties, and RBC ζ-potential. The first group consisted of plasma-only samples and was used to evaluate the viscosity of the surrounding RBC medium. Plasma was obtained from the initial centrifugation of whole blood samples. The second group included RBCs (4% Hct), with or without an oxidative agent, diluted in plasma (1:5000), for the measurement of their viscoelastic properties and bending dynamics. The third group contained a mixture of oxidant-treated and untreated RBCs, diluted in PBS (1:1000), and was used to determine RBC ζ-potential via electrophoretic mobility measurements. Samples without oxidant treatment served as control references.

We chose plasma as the suspending medium for viscoelastic and bending dynamics measurements because it closely reflects the physiological conditions in which RBCs operate, providing a biologically relevant context for studying their mechanical properties. This environment preserves the influence of plasma proteins, electrolytes, and other solutes that are essential for maintaining cellular structure and function. In contrast, PBS was selected as the medium for ζ-potential measurements because its well-defined viscosity, ionic strength, and dielectric constant create a controlled and reproducible environment. Therefore, PBS enables accurate characterization of the electrokinetic behavior of RBCs, without the variability introduced by plasma components, in accordance with established protocols for RBC electrophoresis measurements.[42,43]

2.3. IROS Measurements and Morphological Alterations

Intracellular reactive oxygen species, expressed as the oxidative stress index, were quantified using flow cytometry analysis. For this purpose, RBC suspensions were incubated for 1 h at 37 °C, under gentle agitation, with 2′,7′-dichlorofluorescein diacetate (DCFDA) prepared in PBS-glucose, supplemented with 0.1% bovine serum albumin (BSA). Negative controls were processed without the addition of DCFDA. After incubation, a small volume of 4% RBC suspension was transferred into cytometry tubes prefilled with 0.1% PBS-glucose-BSA buffer. All samples were analyzed via flow cytometry (FACSCanto II, BD Bioscience) and data were processed using FACSDiva software. In parallel to flow cytometric analysis, oxidant-treated and control samples were microscopically examined to evaluate potential morphological changes of RBCs, including reversible and irreversible alterations, as indicators of oxidative damage.

2.4. Overall Elasticity Measurements

We measured the overall elasticity of the cells with the optical tweezer apparatus. Individual optically trapped RBCs were subjected to plasma flow by translating the sample chamber in the x-direction at a constant velocity v (Inset Figure 1), for a total displacement of 200 μm. The trapping laser power was maintained at P = 20 mW at the sample plane to avoid photodamage of the cells.[44] The overall elasticity, μ, of each cell was determined by measuring the elongated cell length, L, during plasma translation as a function of drag velocity, v, using the equation:[10]

$$L = L_0 + \left(\frac{\eta L_0^2}{\mu Z_{eq}}\right) v \quad (1)$$

where, η denotes the plasma dynamic viscosity, L_0 is the initial RBC length, and $1/Z_{eq} = 1/Z_1 + 1/Z_2$ describes the relative distance of the trapped cell from the bottom of the Neubauer chamber (Z_1) and the cover glass (Z_2) (Inset Figure 1). The longitudinal position of the optical trap was set at $Z_1 = Z_2 = 50$ μm using the z-axis of the 3D translation stage. Experiments were performed at plasma translation velocities ranging from 12.5 to 50 μm/s, at increments of 6.25 μm/s. For each donor (n = 10), four samples were prepared (one control and three subjected to different oxidative agents) and ∼10 RBCs were measured per sample. The elongation L of each cell at each drag velocity was determined with an image analysis software (ImageJ, 1.53v). The plasma kinematic viscosity, η_{kin}, was measured at room temperature for each donor, using an Ostwald microviscometer.[45] Knowing the plasma density (ρ) and kinematic viscosity, the dynamic viscosity was then obtained as $\eta = \rho \cdot \eta_{kin}$,[46] assuming blood plasma is modeled as a Newtonian fluid[47,48] with a constant dynamic viscosity, which represents a standard approximation in optical manipulation of RBCs. Indeed, the Ostwald viscometer operates at a shear rate of ∼286 s^{-1} and the RBCs in the optical tweezer experience a shear rate of 0.27–1.09 s^{-1} during dragging (Section S1 of the Supporting Information). In the absence of suspended RBCs or other cellular elements, plasma exhibits no shear-thinning behavior or viscoelasticity within these shear rate regimes and its dynamic viscosity remains constant in this range.

https://doi.org/10.1021/acsabm.6c00869
ACS Appl. Bio Mater. XXXX, XXX, XXX–XXX

The overall elasticity measurements were performed exclusively on the RBC subpopulations that retained a normal, smooth biconcave morphology. Cells exhibiting severe oxidative distortions, such as echinocytes or acanthocytes, were intentionally excluded from these measurements, as their surface irregularities violate the geometric boundary conditions required for the mechanical model employed here (eq 1). It is important to emphasize that the parameter μ derived from this hydrodynamic dragging method represents an apparent overall elasticity metric of the entire RBC acting as an integrated structural unit rather than the intrinsic membrane shear modulus, typically measured via static or localized point-deformation methods, such as dual-trap optical stretching.[49] The global parameter μ inherently integrates the coupled contributions of the membrane shear elasticity, local bending resistance, global cellular geometry, and the viscous effects of internal cytoplasm. A detailed physical analysis and a step-by-step derivation of the force-balance equation underlying the calculation of this parameter are provided in Supporting Information, Section S2.

2.5. Bending Dynamics Measurements

For each donor ($n = 10$), 10 RBCs were measured for each sample (control and subjected to different oxidative agents). In these measurements, the trapping laser power varied from 10 to 50 mW at increments of 10 mW. For each RBC, we aligned the cell center of symmetry with the focal spot of the trapping laser beam to ensure reproducibility of the measurements. Similar to the overall elasticity measurements described in Section 2.4, bending measurements and analysis were exclusively applied to RBCs with undistorted morphology. Severely deformed cells (echinocytes and acanthocytes) were systematically omitted from the bending measurements to avoid structural artifacts caused by altered membrane curvatures.

2.6. ζ-Potential Measurements

The ζ-potential of untreated RBCs (control) and those subjected to oxidative agents was determined using phase analysis light scattering (PALS) with a Zetasizer Nano ZS analyzer (Malvern Instruments, UK). Measurements were carried out at room temperature in a U-shaped capillary cell (DTS1070).[43,50] The ζ-potential was calculated from the measured electrophoretic mobility (u), using the Smoluchowski equation:[51]

$$\zeta = u\eta/\varepsilon \tag{2}$$

where η is the dynamic viscosity and ε the dielectric permittivity of the PBS surrounding medium ($\eta = 0.8882$ cP and $\varepsilon = 79$).[52]

3. RESULTS AND DISCUSSION

3.1. Oxidative Stress-Induced Changes in RBC iROS Levels, Morphology, and ζ-Potential

All three oxidizing agents induced a statistically significant increase in iROS levels compared to untreated controls ($p < 0.01$). In control RBCs, the mean fluorescence intensity (MFI) was 522.5, whereas exposure to t-BHP and diamide resulted in moderate increases to 666.9 and 853.6, respectively. PHZ caused a dramatic elevation in iROS (mean MFI = 7215), an order of magnitude higher than t-BHP and diamide. (Figure 2). These findings support the established role of these agents in promoting oxidative stress in RBCs.[23,53]

All oxidants induced marked alterations in RBC morphology (Figure S2). Acanthocyte formation was significantly increased compared to controls ($p < 0.01$), rising from 0.93% in untreated cells (control) to 19.70% in cells treated with t-BHP, 18.18% with diamide, and 39.34% with PHZ, the latter exerting the strongest effect (Figure 3A). Similarly, echinocyte formation was significantly elevated ($p < 0.01$), from 0% in

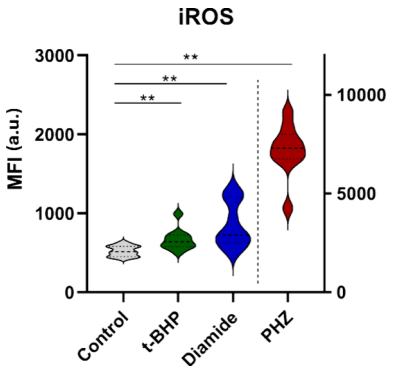

Figure 2. Violin plots showing the distribution of mean fluorescence intensity (MFI) values for control RBCs, as well as those exposed to t-BHP, diamide, and PHZ. MFI values after treatment with PHZ are displayed using a secondary y-axis on the right side, due to their higher range. Statistical significance between paired groups was determined using the Wilcoxon matched-pairs signed-rank test (**$p < 0.01$).

controls to 2.29% with t-BHP, 2.63% with diamide, and 10.54% with PHZ (Figure 3B). In parallel, all oxidants significantly reduced RBC diameter ($p < 0.01$), indicating profound structural remodeling of the cell membrane under oxidative stress (Figure 3C). These morphological changes are in line with previous reports describing oxidant-induced RBC deformation and support the established role of oxidative stress in RBC membrane remodeling.[54]

No significant variations were observed in RBC ζ-potential following treatment with any of the oxidants (Table 1 and Figure 4). The ζ-potential is critical for proper cell function and the prevention of aggregation. In control RBCs, the ζ-potential averaged (−11.31 ± 0.28) mV, consistent with previously reported RBC values.[55] Exposure to t-BHP (−11.5 ± 0.5) mV and diamide (−11.7 ± 0.4) mV produced values that were not statistically different than controls. PHZ induced a slight shift to (−11.9 ± 0.3) mV, however, this variation falls within the experimental error range and is not considered meaningful. Therefore, transmembrane surface charge is found relatively resistant to moderate oxidative stress under the controlled ionic conditions of the PBS buffer. However, the screening effects of plasma proteins and competitive macromolecular adsorption could potentially modulate the effective net charge, meaning that future studies are required to investigate the electrical properties of oxidatively stressed RBCs directly within plasma solution, which closely reflects the physiological circulatory environment. The absence of substantial ζ-potential changes, despite pronounced increases in iROS and clear morphological changes, suggests that the outer electrokinetic surface of RBCs was not markedly affected under the present experimental conditions. This may reflect preferential oxidation of hemoglobin, membrane lipids, and cytoskeletal or membrane-associated proteins.[14,56] however, the glycocalyx and sialic-acid-rich surface layer that largely determine erythrocyte electrophoretic mobility remain relatively preserved.[57] Additionally, the ζ-potential measurements were carried out in PBS, where ionic strength and electrostatic screening may reduce sensitivity to subtle surface-charge changes.[58] Unchanged ζ-potential indicates that oxidative stress can affect RBC mechanics and morphology without causing corresponding changes in the observed surface charge, not that overall membrane integrity has been retained.[15]

https://doi.org/10.1021/acsabm.6c00869
ACS Appl. Bio Mater. XXXX, XXX, XXX−XXX

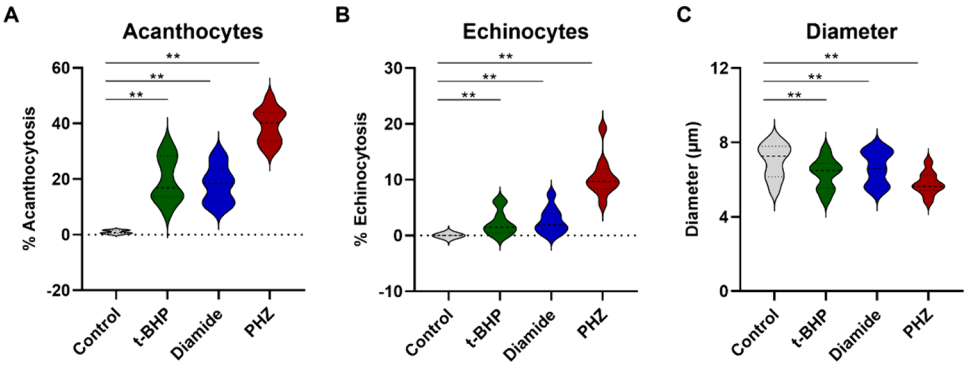

Figure 3. Violin plots showing the distribution of RBC morphological alterations after treatment with different oxidants (t-BHP, diamide, PHZ), compared to untreated controls. (A) Percentage of acanthocytes, (B) percentage of echinocytes, and (C) RBC diameter. Statistical significance between paired groups was determined using the Wilcoxon matched-pairs signed-rank test (**$p < 0.01$).

Table 1. ζ-Potential of Individual Donor RBCs[a]

	ζ-potential [mV]			
donor	control	t-BHP	diamide	PHZ
1	−10.1	−9.55	−10.3	−11.3
2	−11.9	−12.4	−10.9	−12.7
3	−12.3	−12.4	−12.3	−12.5
4	−11.5	−10.5	−12.0	−11.9
5	−10.4	−13.4	−10.3	−12.5
6	−12.0	−9.6	−12.7	−10.8
7	−10.7	−9.52	−11.8	−11.9
8	−10.1	−10.6	−9.75	−11.5
9	−12.0	−13.7	−12.5	−10.1
10	−12.1	−12.9	−14.2	−13.7
average value	−11.31 ± 0.28	−11.5 ± 0.5	−11.7 ± 0.4	−11.9 ± 0.3

[a]The error of each measurement is ± 0.1 mV.

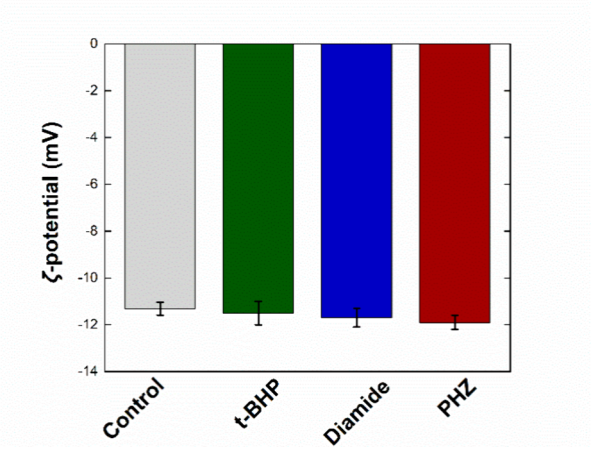

Figure 4. RBC ζ-potential after treatment with oxidants (t-BHP, diamide, PHZ) compared to untreated controls. Displayed values are average values extracted in Table 1.

3.2. Mechanical Properties of RBCs under Oxidative Stress

3.2.1. RBC Elasticity. Individual RBC elasticity under oxidative stress is measured by optical tweezers as described in Section 2. Each optically trapped RBC is subjected to a controlled flow of the surrounding plasma medium and its elongation for different drag velocities is measured, which leads to the derivation of cell elasticity. Figure 5A shows representative elongations of an optically trapped RBC for different plasma drag velocities. For each RBC, a plot of cell elongation as a function of plasma drag velocity is created (Figure 5B) and from the slope of this curve and eq 1, the overall cell elasticity, μ, is obtained. In order to apply eq 1, the plasma dynamic viscosity, η, is determined independently for each donor, as described in Section 2.4 (Table S1 and Figure S3), yielding values consistent with literature findings.[36] The results for RBCs treated with oxidizing agents, as well as control RBCs, are shown in Figure 5C,D. In Figure 5C, the elasticity values reported for each case are the average values of 10 donors, including measurements of ∼10 RBCs for each donor (Table 2). For the untreated RBC population (control group) employed in this study, the average overall elasticity is $\mu = (1.85 \pm 0.14) \times 10^{-4}$ dyn/cm, which is very similar to the average elasticity of RBCs treated with t-BHP ($(1.95 \pm 0.17) \times 10^{-4}$ dyn/cm). These results indicate that t-BHP treatment does not induce significant alterations in RBC membrane elasticity. Diamide results in a statistically significant increase in overall membrane elasticity ($\mu = (2.90 \pm 0.22) \times 10^{-4}$ dyn/cm), $p < 0.01$, indicating that this agent induces oxidative cross-linking of cytoskeletal proteins, resulting in an increased membrane shear modulus and thus membrane stiffening. This mechanical stiffening is associated in general with reduced RBC deformability.[20] In the case of PHZ, a reliable estimation of membrane elasticity was not possible. The excessive oxidative stress caused by PHZ, which is known to induce haemolytic injury,[18] led to profound structural damage of the RBC membrane (Figure S4), which not only impaired the ability of the cells to elongate but also rendered them prone to escape from the optical trap during plasma flow. To address these limitations in future studies, either cell handling should be modified, e.g., by attaching dielectric beads to the cell membrane and using these as trapping handles, or non-Gaussian trapping beams should be employed.

The elasticity measurements correlate with the magnitude of intracellular oxidative stress, as determined in Section 3.1. Indeed, t-BHP induces a moderate increase in iROS, which is associated with preserved overall RBC elasticity, whereas diamide induces a higher increase in iROS, accompanied by increased elasticity. On the other hand, the extreme iROS levels induced by PHZ lead to severe structural damage, preventing reliable elasticity quantification. These oxidant-specific mechanical responses likely arise from the distinct biochemical targets

https://doi.org/10.1021/acsabm.6c00869
ACS Appl. Bio Mater. XXXX, XXX, XXX−XXX

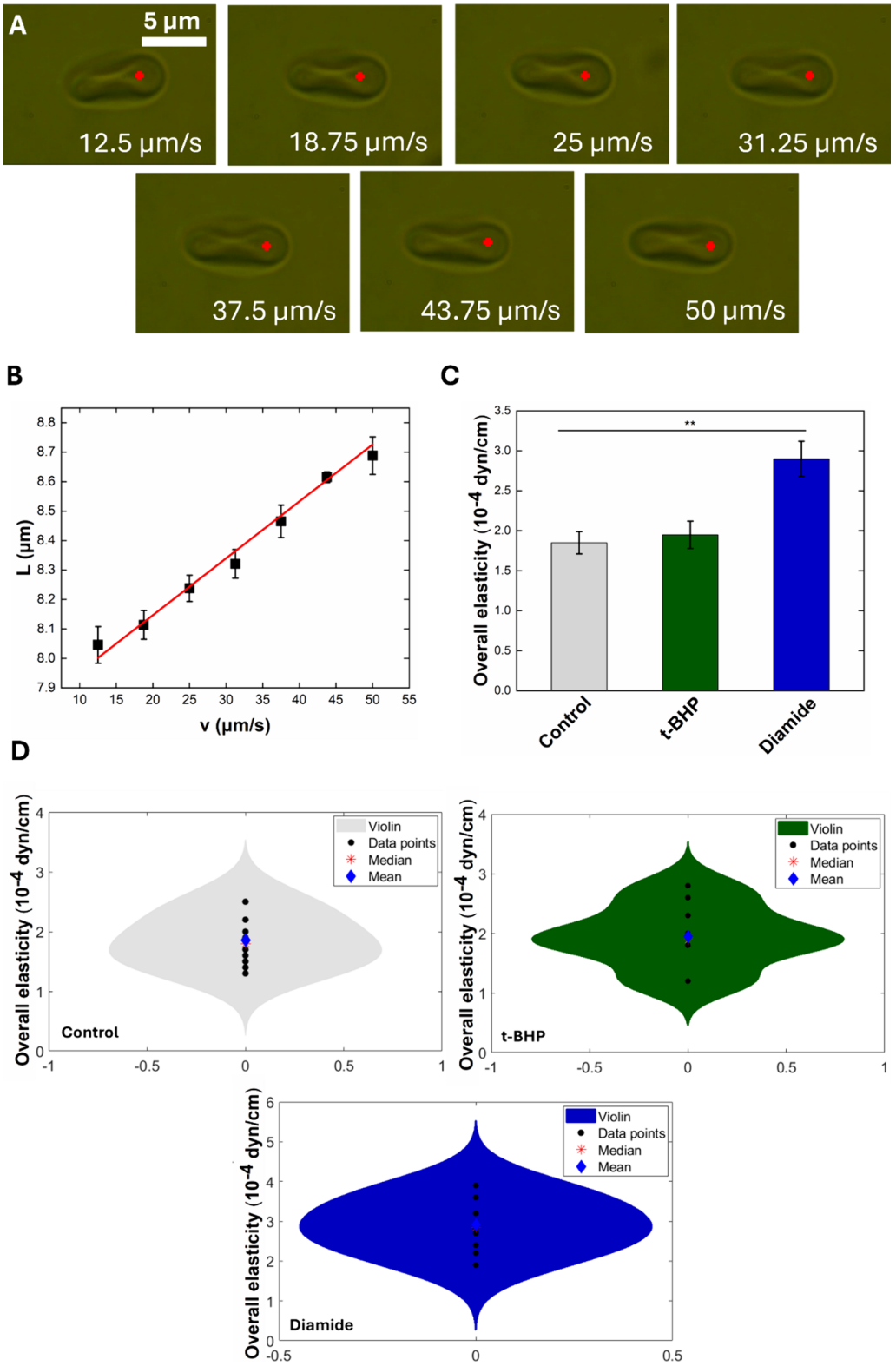

Figure 5. (A) Different elongations of an optically trapped RBC for a range of plasma drag velocities from 12.5 to 50 μm/s. The red cross indicates the focus of the trapping laser beam. (B) Representative plot of a trapped RBC's elongation as a function of plasma drag velocity. (C) Overall RBC elasticity after treatment with oxidants (t-BHP and diamide) compared to untreated controls. Reported values are average for 10 donors and ∼10 RBCs per donor. Statistical significance between paired groups was determined using the Wilcoxon matched-pairs signed-rank test (**$p < 0.01$). (D) Violin plots showing the distribution of the overall elasticity values for control RBCs, as well as those exposed to t-BHP and diamide. Each data point corresponds to the average elasticity value of each donor, for ∼10 RBCs per donor. Horizontal axes indicate the kernel density distribution of the data.

https://doi.org/10.1021/acsabm.6c00869
ACS Appl. Bio Mater. XXXX, XXX, XXX–XXX

Table 2. Overall RBC Elasticity Values for Individual Donors[a]

	overall elasticity [$\times 10^{-4}$ dyn/cm]		
donor	control	t-BHP	diamide
1	1.4 ± 0.3	1.2 ± 0.4	3.2 ± 1.4
2	1.9 ± 0.4	1.8 ± 0.4	1.9 ± 0.4
3	2.0 ± 0.5	1.2 ± 0.3	2.7 ± 0.5
4	1.3 ± 0.2	1.8 ± 0.2	2.2 ± 0.4
5	2.2 ± 0.2	2.8 ± 0.4	2.9 ± 0.5
6	2.5 ± 1.1	2.0 ± 0.4	2.1 ± 0.4
7	1.6 ± 0.4	1.8 ± 0.4	3.9 ± 1.0
8	1.5 ± 0.2	2.6 ± 0.3	2.8 ± 0.6
9	1.7 ± 0.4	2.0 ± 0.3	3.6 ± 0.7
10	2.5 ± 0.6	2.3 ± 0.4	3.6 ± 0.6
# RBCs analyzed	96	101	96
range	1.3–2.5	1.2–2.8	1.9–3.9
average value	1.85 ± 0.14	1.95 ± 0.17	2.90 ± 0.22

[a]For each donor and each oxidizing condition, ∼10 RBCs have been measured.

of each oxidant. t-BHP mainly promotes lipid peroxidation, hemoglobin degradation, and secondary membrane-protein oxidation,[59,60] resulting in mild remodeling without measurable mechanical impairment in morphologically preserved RBCs. Diamide oxidizes erythrocyte membrane sulfhydryl groups and promotes spectrin/cytoskeletal cross-linking,[20,61] explaining the increased apparent overall elasticity and slightly elevated bending modulus. In contrast, PHZ induces hemoglobin oxidation/denaturation, Heinz body formation, band 3 clustering, and membrane destabilization,[62−64] leading to severe morphological distortion and unstable trapping that prevent reliable bending modulus estimation. Therefore, the observed RBC mechanical phenotypes appear to reflect the specific biochemical target of oxidative injury rather than oxidative burden alone.

3.2.2. RBC Bending. Owing to the elastic nature of the RBC membrane, the cells start to bend when they are subjected to gradient optical forces in an optical tweezer system.[9,65] Indeed, in Figure 5A the cell is already folded due to the forces induced by the trapping laser beam, as opposed to an RBC at rest, such as the one shown in Figure S4A. The bending process can be separated into two phases. Initially, the cell exhibits a relative displacement with respect to the focus of the trapping laser beam. When the focus of the trapping laser beam is positioned to the left of the cell's center of symmetry, the cell shifts to the right (Figure 6A), and vice versa. This behavior is similar to the application of an off-center force on a rigid object: when the optical gradient force is applied asymmetrically with respect to the cell's center of symmetry, it generates an effective torque, leading to a displacement of the cell away from the beam focus. Following displacement, RBCs undergo bending due to the optical forces exerted by the laser beam, which deform their flexible membrane. Once the bending process is complete, the cell aligns its major symmetry axis with the polarization direction of the trapping laser beam (Figure 6B).[66] In the experiments performed in this work, the bending behavior of untreated control RBCs and RBCs treated with t-BHP and diamide is similar. In contrast, RBCs treated with PHZ often exhibit highly irregular deformation behavior instead of well-defined bending, characterized by shape collapse and compression, random deformation patterns, and variations from cell to cell, likely due to severe membrane damage and loss of symmetry (Figure S5).

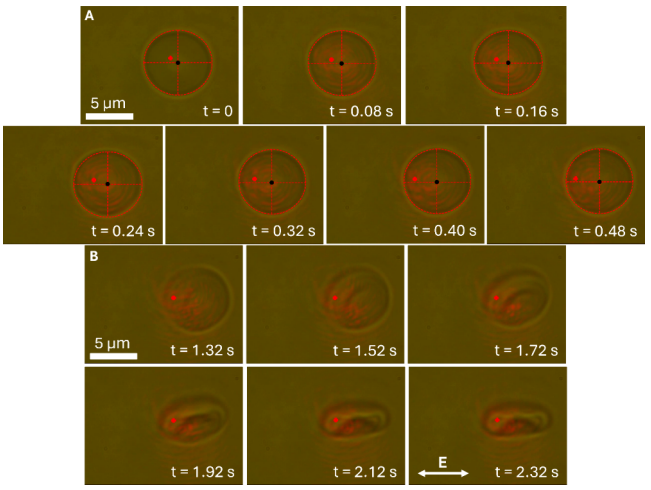

Figure 6. (A) Time lapse of an untreated RBC's relative movement with respect to the trapping laser beam. The red dashed circle indicates the boundary of the cell in the surrounding medium (plasma). The red cross marks the focus of the trapping laser beam, while the black dot indicates the cell's center of symmetry. Irradiation by the laser beam starts at $t = 0$. (B) Time lapse of an untreated RBC bending in the optical tweezer. The white arrow indicates the polarization of the trapping laser beam (incident trapping laser power of 10 mW).

We observe that the bending time, T_{bend}, decreases with increasing trapping laser power, P. Figure 7A shows a representative graph of bending time as a function of the trapping laser power for the control group and for RBCs exposed to t-BHP and diamide, for one donor. The highly irregular behavior of PHZ-treated cells prohibits the extraction of bending dynamics. The bending time is measured from the moment of the opening of the laser shutter until the cell is completely bent. In all cases, bending time decreases with laser power until it reaches a plateau, such that further increase in laser power does not induce significantly faster bending. We model this behavior with the following equation:

$$T_{bend} = \frac{A}{P - P_{min}} + T_{thr} \tag{3}$$

where, T_{thr} represents the minimum bending time of the RBCs, which is not further reduced by increasing the laser power, A is a fitting parameter, and P_{min} is the minimum trapping laser power required for a RBC to bend. Fitting, for each donor, data sets similar to the ones shown in Figure 7A with eq 3, allows us to estimate P_{min}. Knowing P_{min}, the bending modulus, k_c, can be estimated from the following equation:[67]

$$k_c = \frac{fP_{min}s}{c} \tag{4}$$

where, s is the spot size of the trapping laser beam at the focal point, f is the difference in the refractive index of the RBC and the surrounding plasma solution ($n_{RBC} = 1.4$,[68] $n_{plasma} = 1.351$),[69] and c is the speed of light. The spot size produced by the objective lens in the optical tweezer setup is calculated as $s = 542$ nm by the equation $s = 2\lambda/(\pi NA)$.[70] The results

https://doi.org/10.1021/acsabm.6c00869
ACS Appl. Bio Mater. XXXX, XXX, XXX−XXX

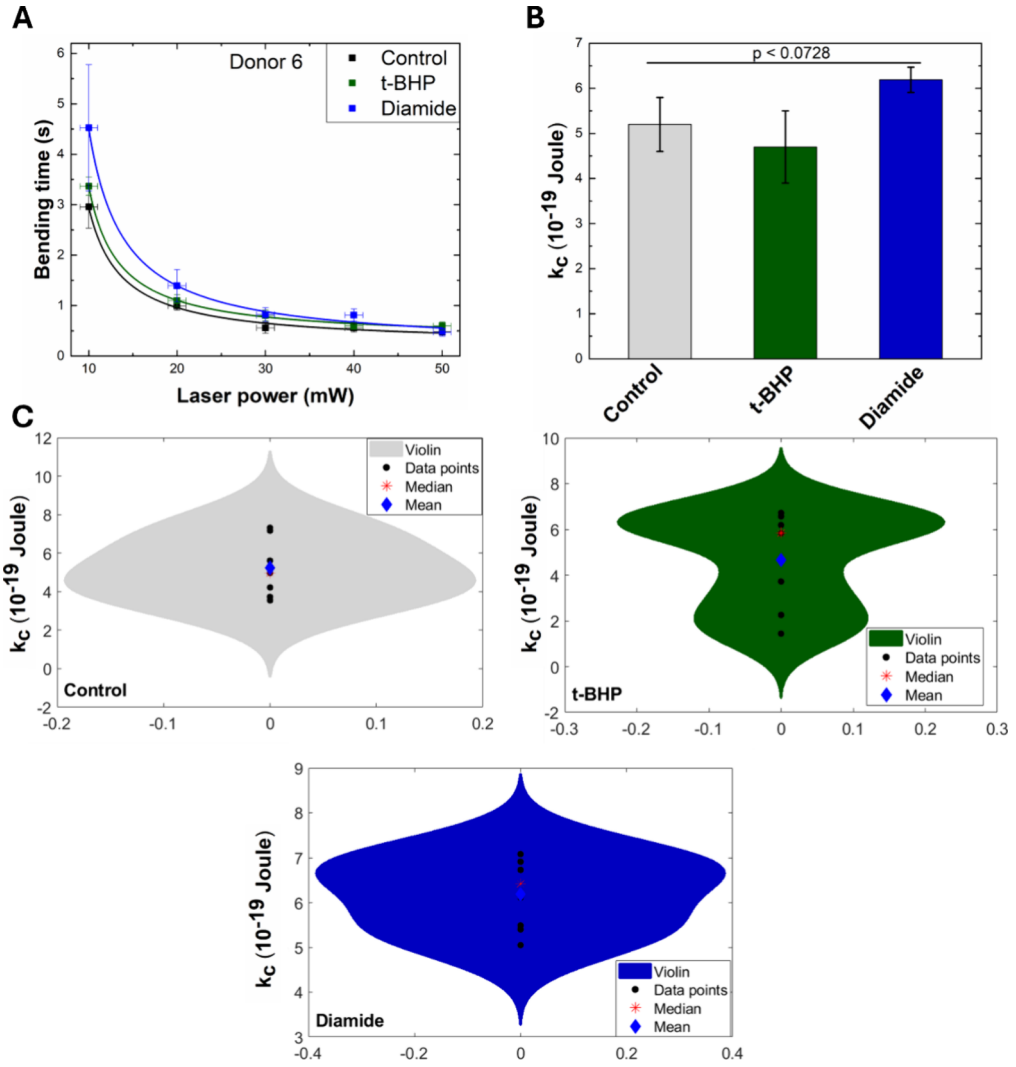

Figure 7. (A) Representative graph of the bending time of optically trapped RBCs from one donor, either control or treated with oxidative agents, as a function of incident trapping laser power. Solid lines correspond to data fits with eq 3. (B) Bending modulus after treatment with oxidants (t-BHP and diamide) compared to untreated controls. Statistical significance between unpaired groups was determined using the Mann-Whitney test ($p < 0.0728$). Reported values are average for 10 donors and ~10 RBCs per donor. (C) Violin plots showing the distribution of the bending modulus values for control RBCs, as well as those exposed to t-BHP and diamide. Horizontal axes indicate the kernel density distribution of the data.

for each donor are shown in Table 3, as average values of measurements on ~10 RBCs for each case (Section 2.5). The average bending modulus of untreated RBCs was measured as $(5.2 \pm 0.6) \times 10^{-19}$ J, while RBCs exposed to t-BHP showed a similar average value of $(4.7 \pm 0.8) \times 10^{-19}$ J. In contrast, cells treated with diamide exhibited a higher average modulus of $(6.19 \pm 0.28) \times 10^{-19}$ J (Figure 7B,C). These trends mirror the overall elasticity results: t-BHP produces minimal changes in both bending modulus and overall elasticity, whereas diamide-treated cells exhibit a modest increase in both parameters, consistent with stiffening of the RBC membrane.[18] Treatment with PHZ induces severe morphological distortions, localized membrane wrinkling, and extensive shape collapse across the cell population. When subjected to optical gradient forces, these aberrant cells exhibit highly irregular, non-reproducible deformation (Figure S5). This unstable behavior arises because the asymmetric geometries of deformed cells and PHZ-induced intracellular aggregates disrupt the optical equilibrium. Consequently, the PHZ-treated group does not satisfy the conditions for applying standard optical bending equations and this subpopulation was excluded from the quantitative bending analysis.

4. CONCLUSIONS

This work demonstrates that oxidative stress exerts distinct and agent-specific effects on the morphology and mechanics of RBCs. All three employed oxidants (t-BHP, diamide, and PHZ) significantly increase intracellular ROS levels and induce morphological alterations, including acanthocytosis, echinocytosis, and reduce cell diameter, consistent with oxidative membrane remodeling. Despite these structural changes, ζ-potential remains largely unaffected, indicating that transmembrane surface charge is relatively resistant to moderate oxidative stress in a standard buffered solution, whereas it remains an open question whether this surface charge preservation persists in

https://doi.org/10.1021/acsabm.6c00869
ACS Appl. Bio Mater. XXXX, XXX, XXX–XXX

Table 3. Bending Modulus, k_c, of Individual Donors[a]

donor	k_c [$\times 10^{-19}$ Joule] control	t-BHP	diamide
1	7.32		
2	7.17	1.44	5.05
3			5.49
4	4.22	6.19	6.91
5	3.73	6.72	6.11
6	5.61	5.83	5.40
7		3.72	6.73
8	3.55	2.26	
9	4.97		6.73
10		6.57	7.08
# RBCs analyzed	96	96	99
range	3.55−7.32	1.44−6.72	5.05−7.08
average value	5.2 ± 0.6	4.7 ± 0.8	6.19 ± 0.28

[a]For each donor and each oxidizing condition, ∼10 RBCs have been measured.

physiological conditions for RBCs. Mechanical probing using optical tweezers reveals that t-BHP exposure does not significantly alter overall elasticity or bending modulus compared with controls, confirming that mild oxidative stress preserves RBC mechanical properties. Diamide treatment, however, enhances overall elasticity and slightly increases bending modulus, suggesting that cross-linking of cytoskeletal proteins may stiffen certain membrane components. On the other hand, PHZ causes severe oxidative injury, manifested by extreme iROS accumulation accompanied by loss of trapping stability, which reflect a profound disruption of the membrane-cytoskeleton complex. Importantly, the values measured for untreated cells were consistent with literature reports for healthy RBCs, validating the accuracy of this approach. Taken together, these results highlight the power of optical trapping, combined with ζ-potential measurements, to provide mechanistic insights into how oxidative stress modulates RBC biophysical properties. By simulating pathological and aging-related damage in a controlled setting, this integrative methodology offers a valuable framework for advancing our understanding of RBC biomechanics in health and disease.

■ ASSOCIATED CONTENT

Data Availability Statement

Data underlying the results presented in this paper are not publicly available at this time but may be obtained from the authors upon reasonable request.

Supporting Information

The Supporting Information is available free of charge at https://pubs.acs.org/doi/10.1021/acsabm.6c00869.

(Section S1) Shear rate calculations; (Section S2) Mathematical derivation of the overall elasticity parameter; (Section S3) Additional figures and tables, as mentioned in the text; (Figure S1) Geometrical model of the RBC; (Figure S2) Oxidant-induced RBC morphological transformations, i.e., acanthocytosis and echinocytosis. Representative brightfield optical microscope images of RBCs following exposure to t-BHP, diamide, or PHZ, as well as control samples. Acanthocytosis: irregularly spiculated RBCs with asymmetric membrane projections. Echinocytosis: crenated RBCs with more uniformly distributed membrane spicules. Images illustrating distinct oxidative stress−dependent remodeling of RBC membrane architecture; (Figure S3) Violin plot showing the distribution of the plasma viscosity of the donors. Horizontal axis indicating the kernel density distribution of the data; (Figure S4) Representative optical microscopy images of a healthy RBC and an RBC damaged by PHZ; (Figure S5) Time lapse of an RBC treated with PHZ, undergoing irregular deformation in the optical tweezer; (Table S1) Plasma dynamic viscosity values for individual donors (DOCX)

■ AUTHOR INFORMATION

Corresponding Author

Maria Kandyla – *Theoretical and Physical Chemistry Institute, National Hellenic Research Foundation, 48 Vasileos Constantinou Avenue, Athens 11635, Greece;* Email: kandyla@eie.gr

Authors

Theodoros Giannakis – *Theoretical and Physical Chemistry Institute, National Hellenic Research Foundation, 48 Vasileos Constantinou Avenue, Athens 11635, Greece; Department of Physics, National and Kapodistrian University of Athens, University Campus, Zografou, Athens 15784, Greece;* orcid.org/0000-0002-9730-5606

Sotirios P. Fortis – *Laboratory of Reliability and Quality Control in Laboratory Hematology (HemQcR), Department of Biomedical Sciences, School of Health & Welfare Sciences, University of West Attica (UniWA), Egaleo City 12243, Greece*

Maria-Aspasia Kosma – *Laboratory of Reliability and Quality Control in Laboratory Hematology (HemQcR), Department of Biomedical Sciences, School of Health & Welfare Sciences, University of West Attica (UniWA), Egaleo City 12243, Greece*

Evangelos Meletis – *Laboratory of Reliability and Quality Control in Laboratory Hematology (HemQcR), Department of Biomedical Sciences, School of Health & Welfare Sciences, University of West Attica (UniWA), Egaleo City 12243, Greece*

Anastasios G. Kriebardis – *Laboratory of Reliability and Quality Control in Laboratory Hematology (HemQcR), Department of Biomedical Sciences, School of Health & Welfare Sciences, University of West Attica (UniWA), Egaleo City 12243, Greece;* orcid.org/0000-0003-3915-1829

Complete contact information is available at: https://pubs.acs.org/doi/10.1021/acsabm.6c00869

Author Contributions

T.G.: investigation, methodology, formal analysis, data curation, and writing the original draft; S.P.F.: investigation, data curation, and formal analysis; M.-A.K.: investigation and data curation; E.M.: investigation and data curation; A.G.K.: resources, validation, and writing - review and editing; M.K.: conceptualization, methodology, resources, writing-review and editing, supervision, and funding acquisition.

Funding

The open access publishing of this article is financially supported by HEAL-Link.

Notes

Human blood samples were obtained from voluntary donors after written informed consent. The study protocol was approved by the Research Ethics Committee of the National and Kapodistrian University of Athens (Protocol No. 107265, 22/09/2025). All samples were anonymized prior to analysis. The authors declare no competing financial interest.

■ ACKNOWLEDGMENTS

The authors express their gratitude to Dr. M. Zoumpanioti and Dr. G. Sotiroudis for assisting with the zeta potential measurements.

■ ABBREVIATIONS

RBC	red blood cell
PHZ	phenylhydrazine
t-BHP	*tert*-butyl hydroperoxide
ROS	reactive oxygen species
AFM	atomic force microscopy
CW	continuous-wave
PBS	phosphate-buffered saline
iROS	intracellular reactive oxygen species
DCFDA	2′,7′-dichlorofluorescein diacetate
BSA	bovine serum albumin
PALS	phase analysis light scattering
MFI	mean fluorescence intensity

■ REFERENCES

(1) Corrons, J. L. V.; Casafont, L. B.; Frasnedo, E. F. Concise Review: How Do Red Blood Cells Born, Live, and Die? *Ann. Hematol.* **2021**, *100* (10), 2425−2433.

(2) Avram, A.; Mocanu, A.; Tomoaia, G.; Rosoiu, C. L.; Dobrota, C. T.; Florea, D. A.; Tomoaia-Cotisel, M. Unveiling the Complexity of Red Blood Cells: Insights into Structure, Properties and Functions. *Ann. Acad. Rom. Sci. Ser. Biol. Sci.* **2023**, *12* (1), 129−154.

(3) Thiagarajan, P.; Parker, C. J.; Prchal, J. T. How Do Red Blood Cells Die? *Front. Physiol.* **2021**, *12*, No. 655393.

(4) de Oliveira, M. A. S.; Moura, D. S.; Fontes, A.; de Araujo, R. E. Damage Induced in Red Blood Cells by Infrared Optical Trapping: An Evaluation Based on Elasticity Measurements. *J. Biomed. Opt.* **2016**, *21* (7), No. 075012.

(5) Himbert, S.; D'Alessandro, A.; Qadri, S. M.; Majcher, M. J.; Hoare, T.; Sheffield, W. P.; Nagao, M.; Nagle, J. F.; Rheinstädter, M. C. The Bending Rigidity of the Red Blood Cell Cytoplasmic Membrane. *PLoS One* **2022**, *17* (8), No. e0269619.

(6) Hughes, M. P. The Cellular Zeta Potential: Cell Electrophysiology beyond the Membrane. *Integr. Biol.* **2024**, *16*, No. zyae003.

(7) Scharte, M.; Fink, M. P. Red Blood Cell Physiology in Critical Illness. *Crit. Care Med.* **2003**, *31* (12), S651−S657.

(8) Tzounakas, V. L.; Anastasiadi, A. T.; Karadimas, D. G.; Zeqo, R. A.; Georgatzakou, H. T.; Pappa, O. D.; Papatzitze, O. A.; Stamoulis, K. E.; Papassideri, I. S.; Antonelou, M. H.; Kriebardis, A. G. Temperature-Dependent Haemolytic Propensity of CPDA-1 Stored Red Blood Cells vs Whole Blood - Red Cell Fragility as Donor Signature on Blood Units. *Blood Transfus.* **2017**, *15* (5), 447−455.

(9) Giannakis, T.; Fortis, S. P.; Starinskiy, S. V.; Kriebardis, A. G.; Kandyla, M. Evaluating the Viscoelastic Properties and Folding Dynamics of Red Blood Cells Maintained at 4 °C Using Optical Tweezers. *Appl. Phys. B* **2026**, *132* (3), No. 40.

(10) Lima, C. N.; Moura, D. S.; Silva, Y. S. S.; Souza, T. H.; Crisafuli, F. A. P.; Silva, D. C. N.; Peres, J. C.; Cesar, C. L.; de Araujo, R. E.; Fontes, A. Evaluating Viscoelastic Properties and Membrane Electrical Charges of Red Blood Cells with Optical Tweezers and Cationic Quantum Dots − Applications to β-Thalassemia Intermedia Hemoglobinopathy. *Colloids Surf., B* **2020**, *186*, No. 110671.

(11) Liu, J.; Zhang, F.; Zhu, L.; Chu, D.; Qu, X. Mechanical Properties of RBCs under Oxidative Stress Measured by Optical Tweezers. *Opt. Commun.* **2019**, *442*, 56−59.

(12) Thomas, T.; Cendali, F.; Fu, X.; Gamboni, F.; Morrison, E. J.; Beirne, J.; Nemkov, T.; Antonelou, M. H.; Kriebardis, A.; Welsby, I.; Hay, A.; Dziewulska, K. H.; Busch, M. P.; Kleinman, S.; Buehler, P. W.; Spitalnik, S. L.; Zimring, J. C.; D'Alessandro, A. Fatty Acid Desaturase Activity in Mature Red Blood Cells and Implications for Blood Storage Quality. *Transfusion* **2021**, *61* (6), 1867−1883.

(13) Kriebardis, A. G.; Antonelou, M. H.; Stamoulis, K. E.; Economou-Petersen, E.; Margaritis, L. H.; Papassideri, I. S. Storage-Dependent Remodeling of the Red Blood Cell Membrane Is Associated with Increased Immunoglobulin G Binding, Lipid Raft Rearrangement, and Caspase Activation. *Transfusion* **2007**, *47* (7), 1212−1220.

(14) Kriebardis, A. G.; Antonelou, M. H.; Stamoulis, K. E.; Economou-Petersen, E.; Margaritis, L. H.; Papassideri, I. S. Progressive Oxidation of Cytoskeletal Proteins and Accumulation of Denatured Hemoglobin in Stored Red Cells. *J. Cell. Mol. Med.* **2007**, *11* (1), 148−155.

(15) Mohanty, J. G.; Nagababu, E.; Rifkind, J. M. Red Blood Cell Oxidative Stress Impairs Oxygen Delivery and Induces Red Blood Cell Aging. *Front. Physiol.* **2014**, *5*, No. 84.

(16) Diederich, L.; Suvorava, T.; Sansone, R.; Keller, T. C. S.; Barbarino, F.; Sutton, T. R.; Kramer, C. M.; Lückstädt, W.; Isakson, B. E.; Gohlke, H.; Feelisch, M.; Kelm, M.; Cortese-Krott, M. M. On the Effects of Reactive Oxygen Species and Nitric Oxide on Red Blood Cell Deformability. *Front. Physiol.* **2018**, *9*, No. 332.

(17) Antonelou, M. H.; Kriebardis, A. G.; Velentzas, A. D.; Kokkalis, A. C.; Georgakopoulou, S. C.; Papassideri, I. S. Oxidative Stress-Associated Shape Transformation and Membrane Proteome Remodeling in Erythrocytes of End Stage Renal Disease Patients on Hemodialysis. *J. Proteomics* **2011**, *74* (11), 2441−2452.

(18) Berger, J. Phenylhydrazine Haematotoxicity. *J. Appl. Biomed.* **2007**, *5*, 125−130.

(19) Dremza, I. K.; Lapshina, E. A.; Kujawa, J.; Zavodnik, I. B. Oxygen-Related Processes in Red Blood Cells Exposed to Tert-Butyl Hydroperoxide. *Redox Rep.* **2006**, *11* (4), 185−192.

(20) Becker, P. S.; Cohens, C. M.; Lux, S. E. The Effect of Mild Diamide Oxidation on the Structure and Function of Human Erythrocyte Spectrin. *J. Biol. Chem.* **1986**, *261* (10), 4620−4628.

(21) Sinha, A.; Chu, T. T. T.; Dao, M.; Chandramohanadas, R. Single-Cell Evaluation of Red Blood Cell Bio-Mechanical and Nano-Structural Alterations upon Chemically Induced Oxidative Stress. *Sci. Rep.* **2015**, *5* (1), No. 9768.

(22) Rifkind, J. M.; Nagababu, E.; Ramasamy, S.; Ravi, L. B. Hemoglobin Redox Reactions and Oxidative Stress. *Redox Rep.* **2003**, *8* (5), 234−237.

(23) Tzounakas, V. L.; Anastasiadi, A. T.; Karadimas, D. G.; Velentzas, A. D.; Anastasopoulou, V. I.; Papageorgiou, E. G.; Stamoulis, K.; Papassideri, I. S.; Kriebardis, A. G.; Antonelou, M. H. Early and Late-Phase 24 h Responses of Stored Red Blood Cells to Recipient-Mimicking Conditions. *Front. Physiol.* **2022**, *13*, No. 907497.

(24) Xie, Y.; Liu, X. Multifunctional Manipulation of Red Blood Cells Using Optical Tweezers. *J. Biophotonics* **2022**, *15* (2), No. e202100315.

(25) Sokolov, I.; Dokukin, M. E.; Guz, N. V. Method for Quantitative Measurements of the Elastic Modulus of Biological Cells in AFM Indentation Experiments. *Methods* **2013**, *60* (2), 202−213.

(26) Glenister, F. K.; Coppel, R. L.; Cowman, A. F.; Mohandas, N.; Cooke, B. M. Contribution of Parasite Proteins to Altered Mechanical Properties of Malaria-Infected Red Blood Cells. *Blood* **2002**, *99* (3), 1060−1063.

(27) Krishnevskaya, E.; Molero, M.; Ancochea, Á.; Hernández, I.; Vives-Corrons, J.-L. New-Generation Ektacytometry Study of Red Blood Cells in Different Hemoglobinopathies and Thalassemia. *Thalass. Rep.* **2023**, *13* (1), 70−76.

(28) Laurent, V. M.; Hénon, S.; Planus, E.; Fodil, R.; Balland, M.; Isabey, D.; Gallet, F. Assessment of Mechanical Properties of Adherent Living Cells by Bead Micromanipulation: Comparison of Magnetic Twisting Cytometry vs Optical Tweezers. *J. Biomech. Eng.* **2002**, *124* (4), 408−421.
(29) Kotsifaki, D. G.; Kandyla, M.; Lagoudakis, P. G. Near-Field Enhanced Optical Tweezers Utilizing Femtosecond-Laser Nanostructured Substrates. *Appl. Phys. Lett.* **2015**, *107* (21), No. 211111.
(30) Bustamante, C. J.; Chemla, Y. R.; Liu, S.; Wang, M. D. Optical Tweezers in Single-Molecule Biophysics *Nat. Rev. Methods Primers.* **2021**, *1*, No. 25.
(31) Ramser, K.; Hanstorp, D. Optical Manipulation for Single-Cell Studies. *J. Biophotonics* **2010**, *3* (4), 187−206.
(32) Brandão, M. M.; Saad, S. T. O.; Cezar, C. L.; Fontes, A.; Costa, F. F.; Barjas-Castro, M. L. Elastic Properties of Stored Red Blood Cells from Sickle Trait Donor Units. *Vox Sang.* **2003**, *85*, 213−215.
(33) Silva, J. A. X.; Albertini, A. V. P.; Fonseca, C. S. M.; Silva, D. C. N.; Carvalho, V. C. O.; Lima, V. L. M.; Fontes, A.; Costa, E. V. L.; Nogueira, R. A. Biomechanical and Biochemical Investigation of Erythrocytes in Late Stage Human Leptospirosis. *Braz. J. Med. Biol. Res.* **2020**, *53* (8), No. e9268.
(34) Brandão, M. M.; Fontes, A.; Barjas-Castro, M. L.; Barbosa, L. C.; Costa, F. F.; Cesar, C. L.; Saad, S. T. O. Optical Tweezers for Measuring Red Blood Cell Elasticity: Application to the Study of Drug Response in Sickle Cell Disease. *Eur. J. Haematol.* **2003**, *70* (4), 207−211.
(35) Dharmadhikari, J. A.; Roy, S.; Dharmadhikari, A. K.; Sharma, S.; Mathur, D. Torque-Generating Malaria-Infected Red Blood Cells in an Optical Trap. *Opt. Express* **2004**, *12* (6), 1179−1184.
(36) Barjas-Castro, M. L.; Brandão, M. M.; Fontes, A.; Costa, F. F.; Cesar, C. L.; Saad, S. T. O. Elastic Properties of Irradiated RBCs Measured by Optical Tweezers. *Transfusion* **2002**, *42* (9), 1196−1199.
(37) Liu, J.; Zhu, L.; Zhang, F.; Dong, M.; Qu, X. Microdeformation of RBCs under Oxidative Stress Measured by Digital Holographic Microscopy and Optical Tweezers. *Appl. Opt.* **2019**, *58* (15), No. 4042.
(38) Zachariah, E.; Bankapur, A.; Santhosh, C.; Valiathan, M.; Mathur, D. Probing Oxidative Stress in Single Erythrocytes with Raman Tweezers. *J. Photochem. Photobiol., B* **2010**, *100* (3), 113−116.
(39) Jeon, H.-J.; Lee, H.; Yoon, D. S.; Kim, B.-M. Dielectrophoretic Force Measurement of Red Blood Cells Exposed to Oxidative Stress Using Optical Tweezers and a Microfluidic Chip. *Biomed. Eng. Lett.* **2017**, *7* (4), 317−323.
(40) Zhu, R.; Avsievich, T.; Popov, A.; Meglinski, I. Optical Tweezers in Studies of Red Blood Cells. *Cells* **2020**, *9* (3), No. 545.
(41) Blázquez-Castro, A. Optical Tweezers: Phototoxicity and Thermal Stress in Cells and Biomolecules. *Micromachines* **2019**, *10* (8), No. 507.
(42) Sowemimo-Coker, S. O.; Meiselman, H. J. Effect of Procaine Hydrochloride on the Electrophoretic Mobility of Human Red Blood Cells. *Cell Biophys.* **1989**, *15* (3), 235−248.
(43) Bondar, O. V.; Saifullina, D. V.; Shakhmaeva, I. I.; Mavlyutova, I. I.; Kazan, T. I. A. Monitoring of the Zeta Potential of Human Cells upon Reduction in Their Viability and Interaction with Polymers. *Acta Naturae* **2012**, *4* (1), 78−81.
(44) Avsievich, T.; Zhu, R.; Popov, A.; Bykov, A.; Meglinski, I. The Advancement of Blood Cell Research by Optical Tweezers. *Rev. Phys.* **2020**, *5*, No. 100043.
(45) Beaulieu, L. Y.; Logan, E. R.; Gering, K. L.; Dahn, J. R. An Automated System for Performing Continuous Viscosity vs Temperature Measurements of Fluids Using an Ostwald Viscometer. *Rev. Sci. Instrum.* **2017**, *88* (9), No. 095101.
(46) Hutchinson, A. J.; Gusinow, R. J.; Grae Worster, M. The Evolution of a Viscous Gravity Current in a Confined Geometry. *J. Fluid Mech.* **2023**, *959*, No. A4.
(47) Fatahian, E.; Kordani, N.; Fatahian, H. A Review on Rheology of Non-Newtonian Properties of Blood. *IIUM Eng. J.* **2018**, *19* (1), 237−250.
(48) Brust, M.; Schaefer, C.; Doerr, R.; Pan, L.; Garcia, M.; Arratia, P. E.; Wagner, C. Rheology of Human Blood Plasma: Viscoelastic vs Newtonian Behavior. *Phys. Rev. Lett.* **2013**, *110* (7), No. 078305.
(49) Pesen, T.; Haydaroglu, M.; Capar, S.; Parlatan, U.; Unlu, M. B. Comparison of the Human's and Camel's Red Blood Cell Deformability by Optical Tweezers and Raman Spectroscopy. *Biochem. Biophys. Rep.* **2023**, *35*, No. 101490.
(50) Omi, T.; Kajii, E.; Ikemoto, S. The Electrokinetic Behavior of Red Blood Cells from a Patient with Tn Syndrome by Doppler Electrophoretic Light Scattering Analysis. *Tohoku J. Exp. Med.* **1994**, *174* (4), 369−377.
(51) Fontes, A.; Castro, M. L. B.; Brandão, M. M.; Fernandes, H. P.; Thomaz, A. A.; Huruta, R. R.; Pozzo, L. Y.; Barbosa, L. C.; Costa, F. F.; Saad, S. T. O.; Cesar, C. L. Mechanical and Electrical Properties of Red Blood Cells Using Optical Tweezers. *J. Opt.* **2011**, *13* (4), No. 044012.
(52) Kalargyrou, A. A.; Basche, M.; Hare, A.; West, E. L.; Smith, A. J.; Ali, R. R.; Pearson, R. A. Nanotube-like Processes Facilitate Material Transfer between Photoreceptors. *EMBO Rep.* **2021**, *22* (11), No. e53732.
(53) Anastasiadi, A. T.; Paronis, E. C.; Arvaniti, V. Z.; Velentzas, A. D.; Apostolidou, A. C.; Balafas, E. G.; Dzieciatkowska, M.; Kostomitsopoulos, N. G.; Stamoulis, K.; Papassideri, I. S.; D'alessandro, A.; Kriebardis, A. G.; Antonelou, M. H.; Tzounakas, V. L. The Post-Storage Performance of RBCs from Beta-Thalassemia Trait Donors Is Related to Their Storability Profile. *Int. J. Mol. Sci.* **2021**, *22* (22), No. 12281.
(54) Gyawali, P.; Richards, R. S.; Bwititi, P. T.; Nwose, E. U. Association of Abnormal Erythrocyte Morphology with Oxidative Stress and Inflammation in Metabolic Syndrome. *Blood Cells Mol. Dis.* **2015**, *54* (4), 360−363.
(55) Fernandes, H. P.; Cesar, C. L.; de Barjas-Castro, M. L. Electrical Properties of the Red Blood Cell Membrane and Immunohematological Investigation. *Rev. Bras. Hematol. Hemoter.* **2011**, *33* (4), 297−301.
(56) Orrico, F.; Laurance, S.; Lopez, A. C.; Lefevre, S. D.; Thomson, L.; Möller, M. N.; Ostuni, M. A. Oxidative Stress in Healthy and Pathological Red Blood Cells. *Biomolecules* **2023**, *13* (8), No. 1262.
(57) Jan, K.-M.; Chien, S. Role of Surface Electric Charge in Red Blood Cell Interactions. *J. Gen. Physiol.* **1973**, *61* (5), 638−654.
(58) Doltchinkova, V.; Lozanova, S.; Rukova, B.; Nikolov, R.; Ivanova, E.; Roumenin, C. Electrokinetic Properties of Healthy and β-Thalassemia Erythrocyte Membranes under in Vitro Exposure to Static Magnetic Field. *Front. Chem.* **2023**, *11*, No. 1197210.
(59) Trotta, R. J.; Sullivan, S. G.; Stern, A. Lipid Peroxidation and Haemoglobin Degradation in Red Blood Cells Exposed to T-Butyl Hydroperoxide The Relative Roles of Haem- and Glutathione-Dependent Decomposition of t-Butyl Hydroperoxide and Membrane Lipid Hydroperoxides in Lipid Peroxidation and Haemolysis. *Biochem. J.* **1983**, *212* (3), 759−772.
(60) Roy, A.; Sil, P. C. Tertiary Butyl Hydroperoxide Induced Oxidative Damage in Mice Erythrocytes: Protection by Taurine. *Pathophysiology* **2012**, *19* (2), 137−148.
(61) Deuticke, B.; Poser, B.; Lütkemeier, P.; Haest, C. W. M. Formation of Aqueous Pores in the Human Erythrocyte Membrane after Oxidative Cross-Linking of Spectrin by Diamide. *Biophys. Acta, Biomembr.* **1983**, *731* (2), 196−210.
(62) Reinhart, W. H.; Sung, L. P.; Chien, S. Quantitative Relationship between Heinz Body Formation and Red Blood Cell Deformability. *Blood* **1986**, *68* (6), 1376−1383.
(63) Low, P. S.; Waugh, S. M.; Zinke, K.; Drenckhahn, D. The Role of Hemoglobin Denaturation and Band 3 Clustering in Red Blood Cell Aging. *Science (1979)* **1985**, *227* (4686), 531−533.
(64) Schlüter, K.; Drenckhahn, D. Co-Clustering of Denatured Hemoglobin with Band 3: Its Role in Binding of Autoantibodies against Band 3 to Abnormal and Aged Erythrocytes. *Proc. Natl. Acad. Sci. USA* **1986**, *83* (16), 6137−6141.
(65) Dharmadhikari, J. A.; Roy, S.; Dharmadhikari, A. K.; Sharma, S.; Mathur, D. Naturally Occurring, Optically Driven, Cellular Rotor. *Appl. Phys. Lett.* **2004**, *85* (24), 6048−6050.

(66) Dharmadhikari, J. A.; Marthur, D. Using an Optical Trap to Fold and Align Single Red Blood Cells. *Curr. Sci.* **2004**, *86*, 1432−1437.
(67) Ghosh, A.; Sinha, S.; Dharmadhikari, J. A.; Roy, S.; Dharmadhikari, A. K.; Samuel, J.; Sharma, S.; Mathur, D. Euler Buckling-Induced Folding and Rotation of Red Blood Cells in an Optical Trap. *Phys. Biol.* **2006**, *3* (1), 67−73.
(68) Kinnunen, M.; Kauppila, A.; Karmenyan, A.; Myllylä, R.; Park, Y.; Diez-Silva, M.; Fu, D.; Popescu, G.; Choi, W.; Barman, I.; Suresh, S.; Feld, M. S.; Bambardekar, K.; Dharmadhikari, J. A.; Dharmadhikari, A. K.; Yamada, T.; Kato, T.; Kono, H.; Fujimura, Y.; Sharma, S.; Mathur, D. Effect of the Size and Shape of a Red Blood Cell on Elastic Light Scattering Properties at the Single-Cell Level. *Biomed. Opt. Express* **2011**, *2* (7), 1803−1814.
(69) Sumathi, J.; Jaleeli, Z. A.; Jaleeli, K. A.; Ahmad, A. To Investigate the Refractive Index of Blood Plasma Suspended in Various Tonicity Solutions. *J. Res. Appl. Sci. Biotechnol.* **2022**, *1* (3), 216−221.
(70) Starinskiy, S. V.; Giannakis, T.; Chouchoumi, N.; Sulyaeva, V. S.; Tsilipakos, O.; Kandyla, M. Subwavelength Photonic Nanojet Processing of Thin Metal Films Using Optical Tweezers. *Surf. Interfaces* **2025**, *72*, No. 107192.

https://doi.org/10.1021/acsabm.6c00869
ACS Appl. Bio Mater. XXXX, XXX, XXX−XXX